



Oriented granulometry to quantify fibre orientation distributions in synthetic and plant fibre composite preforms

C. Vangsøe, N. Nørskov, M. Devaux, Estelle Bonnin, K. Bach Knudsen

► To cite this version:

C. Vangsøe, N. Nørskov, M. Devaux, Estelle Bonnin, K. Bach Knudsen. Oriented granulometry to quantify fibre orientation distributions in synthetic and plant fibre composite preforms. *Industrial Crops and Products*, 2020, 152 (37), pp.1-7. 10.1016/j.indcrop.2020.112548 . hal-03162857

HAL Id: hal-03162857

<https://hal.inrae.fr/hal-03162857>

Submitted on 22 Aug 2022

HAL is a multi-disciplinary open access archive for the deposit and dissemination of scientific research documents, whether they are published or not. The documents may come from teaching and research institutions in France or abroad, or from public or private research centers.

L'archive ouverte pluridisciplinaire **HAL**, est destinée au dépôt et à la diffusion de documents scientifiques de niveau recherche, publiés ou non, émanant des établissements d'enseignement et de recherche français ou étrangers, des laboratoires publics ou privés.



Distributed under a Creative Commons Attribution - NonCommercial 4.0 International License

Oriented granulometry to quantify fibre orientation distributions in synthetic and plant fibre composite preforms

Victor Gager^{1,2}, David Legland³, Alain Bourmaud¹, Antoine Le Duigou¹, Floran Pierre², Karim Behloul², Christophe Baley¹

⁽¹⁾ Univ. Bretagne Sud, UMR CNRS 6027, IRDL, F-56100 Lorient, France

⁽²⁾ Eco-technilin SAS, ZA Caux Multipôles, 76190 Valliquerville, France

⁽³⁾ UR1268 Biopolymères Interactions Assemblages, INRA, F-44316 Nantes, France

Corresponding author: alain.bourmaud@univ-ubs.fr

Abstract

Fibre orientation is an essential factor governing the mechanical properties of composite materials. This study proposes an original method based on gray-level granulometry to analyse the fibre orientation distribution (FOD) of synthetic and natural fibre reinforcements aiming composite applications. An orientation maps is computed from SEM images and frequency of fibre orientation is graphically illustrated for each angular direction. First, glass fibre nonwoven and unidirectional preforms were analysed as a model to validate the method before testing their flax fibre counterparts. Differences in structural organisations were found between flax and glass fibre reinforcement FOD due to the specific structure and mechanical behaviour of plant fibres but also to the preform manufacturing process. Promising results were obtained confirming the reliability of this novel numerical method for fibre orientation determination.

Keywords: Biocomposites; Preforms; Fibre Orientation Distribution; Flax fibre,
Microstructure analysis; Nonwovens;

1. Introduction

Flax fibres are now widely used as reinforcements for semi-structural and structural composite applications (Shah et al., 2013). Their specificities (low density, good mechanical properties, particular structure, low environmental impact, etc.) make them a very attractive alternative to synthetic fibres (Bourmaud et al., 2018). Flax fibres are commercially available for extrusion, injection moulding or as structured preforms for infusion and compression moulding such as unidirectional, multi-directional woven fabrics and also nonwoven mats. Selection of preforms can be managed depending on the properties and expected end applications. Nonwoven composites are mainly used in the automotive industry as interior parts because they combine good mechanical and acoustic properties (Merotte et al., 2016) but also thanks to their low manufacturing cost compared to fabrics. Composites performances are usually defined by the reinforcement, matrix and fibre/matrix interface properties (Jones, 1999). In terms of mechanical properties, additional parameters such as fibre volume ratio, fibre architecture and individualisation, porosity content as well as fibre orientation are of great importance. For this later, it is even more true when dealing with nonwoven biocomposites where the fibre orientation distribution can be considered as quasi isotropic (Gnaba et al., 2018). Still, depending on the manufacturing method and especially with carding process, they can highlight preferred orientations (Miao and Shan, 2011; Russell, 2007). Also, during a mechanical loading, fibres will be loaded differently depending on the orientation distribution. Due to their structure, flax fibres highlight high anisotropic properties and longitudinal, transverse and shearing properties of flax elementary and technical fibres (bundles) (Baley et al., 2006;

Thomason et al., 2017) that could greatly influence the overall composite's behaviour and properties (Gager et al., 2019; Merotte et al., 2018).

Through research work around the world, there is now a good knowledge based on nonwoven composites, particularly in terms of the influence of the type of reinforcement, their microstructure and their various properties (Martin et al., 2016; Merotte et al., 2016; Mieck et al., 1996). However, to allow optimised structural and semi-structural applications, modelling and designing tools of these materials are required. In terms of modelling mechanical properties, one of the major challenges to be addressed is the implementation of fibre orientation and curvature. To do this, it is necessary to rely on trusted data that can only be determined experimentally from existing preforms.

Several studies have focused on the determination of the fibre orientation distribution for various materials including fabrics, paper or fibre reinforced polymers. Acquisition of images with digital cameras, optical, electronic or confocal microscopes are the most commonly used (Enomae et al., 2006; Erdman et al., 2016; Koh and Madsen, 2018). Miao and Shan (Miao and Shan, 2011) have studied the relationship between fibre orientation and mechanical properties of flax nonwoven composites thanks to optical microscopy imaging and then analysis Fiji[®] image processing software. Other methods such as ultrasound scanning and X-ray Computed tomography were used by Smith et al. to create 3D representations of carbon fibre composite plates (Smith et al., 2015). From synchrotron radiation-based micro-computer tomography, Graupner et al. (Graupner et al., 2016, 2014) characterised the fibre orientation of cellulose fibre-reinforced polylactide composites by analysing the in-plane fibre orientations of several slices through the thickness of the composite. All acquisition techniques can be justified depending on the aim of the observation afterward. Indeed, different methods will allow to get 2D or 3D images, characterise diverse surface areas from micro to macro scale,

with more or less precision and contrasts. Some techniques are also more suitable for the analysis methods through which they will then be computed to determine the orientation of the fibres (i.e. gray level or colour images) (Syerko et al., 2019).

Methods applicability must also be evaluated depending on the morphology of the reinforcing fibres. Depending on the required performances and on their final use application, composites can be reinforced with short or continuous fibres. For the first category, the fibre orientation will mainly be a result of the flow of the suspension within the polymer during the process. For long, continuous fibre composites, the orientation will be given by the structure of the preform (i.e. woven fabrics, nonwoven preforms etc..) as well as the structure of the long fibres which will govern their straightness. Plant fibre reinforcement potentially being made of both bundles or individual fibres (Baley et al., 2019); diameters are also of great importance. Thus, to be consistent, fibre orientations quantification methods must correctly identify the reinforcing elements (individual fibres, bundles) as well as their curvature and take the fibre morphological characteristics (diameter and length) into account.

The main method used to determine the fibre orientation distribution in long fibre reinforced composites is the Fast Fourier Transform (FFT) whose efficiency is discussed in the literature (Ghassemieh et al., 2002; Pourdeyhimi and Kim, 2002). Due to the periodic character of the Fourier transformation, this method is useful to describe regular patterns in woven fabric where information is concentrated in the Fourier spectrum in the vertical or horizontal direction, respectively. In contrast, purely random orientation of fibres causes the frequency components in the power spectrum to be approximately isotropic and possess a nearly circular shape (Yousfani et al., 2012). Tunák et al. (Tunák et al., 2014; Tunák and Antoch, 2018) highlighted that the "global" approach commonly used was not suitable enough to analyse nonwoven textiles or nanofibrous layers, which often present non-homogeneity as well as anisotropy, and that

further detailed analysis were more convenient. By automatically splitting the image into several small sub-images and analysing them, they increased the efficiency of the determination of the (fibre orientation distribution) FOD for textiles with several peaks of orientations. However, results obtained with FFT based methods are very dependent of the applied algorithms and smoothing filters (Kratmann et al., 2009). Furthermore, this method needs a strong contrast between the background and the fibres which works relatively well with fibres such as polymeric or metallic and synthetic fibres. In the case of natural fibres, contrast can vary significantly, even one a singular fibre, because of its structure and biochemical composition which may bias the results. Other methods such as the stereological method can be used; the composite is observed in its crossed direction and the orientation of a circular fibre is determined from the ratio of the ellipse formed by the orientation of a fibre (Eberhardt and Clarke, 2001; Jeon et al., 2014; Yurgartis, 1987). This method does work for circular diameter fibre such as a glass fibre but it cannot be applied to plant fibres which present complex heterogeneous structures. Furthermore, as it is only at one location in the in-plane direction, curvature of the fibre cannot be determined. Local gradient orientation method can also be used but this way is questionable as only fibre edges are detected by filtering operators which means fibre widths are not taken into account and this is a predominant information when dealing with plant fibres. Other methods such as structure tensor (Krause et al., 2010; Van Kempen et al., 1999) or mean intercept length (Luo et al., 1991; Sander and Barocas, 2009) methods were also applied on composite materials and each of them has its own benefits and drawback from the complexity to the accuracy of the method (Syerko et al., 2019).

Despite their applicability to analyse composite materials, the methods previously enounced are usually programmed in operating systems/software for which it is not possible to manage settings such as the time of calculation and the accuracy of the results. Also, depending on the applications, there is a need of a method where such

parameters can be managed. For scientific matters, the accuracy of the results is prevalent. From an industrial point of view, a method quantifying the fibre orientation in a preform directly after the production in order to control its conformity might be of great interest. For this purpose, even if accuracy is important, the time of calculation is a predominant factor if there is a large area to analyse. Moreover, by developing a method for which there is a full understanding of the protocol, it is easier for the developers to modify calculation algorithms to make them more efficient according to the material characteristics.

This paper presents an original method based on gray-level granulometry to analyse the fibre orientation distribution of both synthetic and flax preforms for composite reinforcement. After a validation of the method developed on glass fibres unidirectional (UD) and nonwoven preforms, results obtained with similar flax fibre preforms are shown and discussed.

2. Materials and methods

2.1 Materials

Flax (*Linum usitatissimum*) tows and scutched fibres grown in Normandy (France) were used to produce the nonwoven and the unidirectional tape (Martin et al., 2014). Natural fibre nonwovens were manufactured according to the carding/over-lapping/needle punching technology (Russell, 2007) whereas the unidirectional tape is produced by a specific process well described by Khalfallah et al. (Khalfallah et al., 2014). The materials (i.e. nonwoven and UD tape), coming from Eco-Technilin SAS®, have an areal weight of respectively 70 g.m⁻² and 110 g.m⁻², respectively. E-Glass fibre mat and unidirectional fabric made respectively following air blowing (Russell, 2007) and weaving technologies were also studied to validate the method. They were supplied by Composite Distribution and have both an areal weight of 200 g.m⁻². The unidirectional

fabric is not a pure UD fabric as it presents a few fibres in the weft direction (weight fraction around 0.4%). Names and properties related to the different preforms are given in table 1.

Table 1. Characteristics of the various preforms analysed.

Name	Type	Fibre type	Areal weight (g/m ²)	Preform thickness (μm)	Fibres/bundles length (mm)	Preferred orientation (°)
Flax UD	Unidirectional	Flax	70	150 ± 20	Bundles assembly	Longitudinal
Flax NW	Nonwoven	Flax	110	200 ± 10	50-200	Cross direction (CD)
Glass UD	Unidirectional	Glass	200	190 ± 20	continuous	Longitudinal
Glass mat	Nonwoven	Glass	200	460 ± 40	40-70	None

2.2 Scanning Electronic Microscope Imaging

SEM observations were performed on glass and flax preforms. Rectangular samples (60x40 mm) were sputter-coated with a thin layer of gold in an Edwards Sputter Coater and analysed with a Jeol JSM 6460LV SEM at 20 kV.

2.3 Images Analysis Methodology

Images were analysed by computing the histogram of the preferred orientation of pixels. The preferred orientation is computed by applying gray-level granulometry curves with various orientations, computing a typical size in each direction, and estimating the preferred orientation from typical sizes.

Figure 1.

Gray-level granulometry is an approach for image texture analysis based on the application of morphological filters (typically opening or closing) of increasing size (Devaux et al., 2008; Soille, 2003). Gray-level morphological opening is an operation that removes bright structures that are smaller than the structuring element. Let us denote by $\gamma_B(I)$ the result of morphological opening with structuring element B_λ of size λ on the image I . The computation of granulometry involves a family of structuring elements

177 $\{B_{\lambda_i}\}_{i=1,\dots,n}$ of increasing sizes λ_i . The result obtained with each size λ_i is summarised by
 178 the image volume curve V_i , that corresponds to the sum of the gray level values in the
 179 corresponding result of opening. The derivative of the image volume curve results in
 180 granulometric curves that can be interpreted in terms of size distribution:

$$181 \quad G_i = \frac{V_{i+1} - V_i}{V_{\infty} - V_0}$$

182 Figure 1 presents an example of granulometric curve computed on a sample image of a
 183 flax fibres nonwoven. A peak can be noticed around 5 pixels, that corresponds to the
 184 thickness of the majority of fibres visible in image. Another peak can be noticed around
 185 15 pixels, corresponding to thicker fibres. The corresponding fibres are visible on the top
 186 images.

187 A granulometric curve can be summarised by a gray-level mean size that depicts the
 188 typical size of the structures within the image. The geometrical mean $m_G =$
 189 $\exp[\sum_i \log \lambda_i G_i]$ was considered, which resulted in values closer to the centre of the peak
 190 than the mean or the median (Devaux et al., 2008).

191 Gray-level granulometry is typically computed using structuring elements with square or
 192 disk shapes. In order to assess the preferred orientation of texture, linear structuring
 193 elements with various orientations may be used (Devaux et al., 2008; Legland et al.,
 194 2012; Soille, 2003). Families of linear structuring elements were considered; they are
 195 obtained by identifying the pixels around the line with orientation θ containing the origin,
 196 and keeping the number of pixels that best approximates the expected length. The
 197 computation of granulometric curves on the whole image using linear structuring
 198 elements with various orientations results in a granulometric curve for each orientation.
 199 The computation of geometric means results in a function $m_G(\theta)$ that depicts the typical
 200 size depending on the orientation.

201 **Figure 2.**

In order to compute preferred orientation for a given pixel, it is necessary to compute locally (i.e. for each pixel) the functions $m_G(\theta)$. In practice, this requires to replace the computation of global image volumes V_i by their local counterparts $V_i(x, \theta)$, where x corresponds to the pixel position and θ corresponds to the orientation. Resulting granulometric curves $G_i(x, \theta)$ can be summarised by computing for each pixel and for each orientation the local oriented gray-level mean size $m_G(x, \theta)$. Fig. 2.B and Fig. 3.C show examples of local gray-level mean size maps for orientations corresponding to 0, 45, 90, and 135 degrees computed on a synthetic image (Fig. 2.A) and on a cropped image of flax fibres (Fig. 3.A). The elongated regions result in a large mean size value when the orientation corresponds to the orientation of elongation.

For each pixel, the function $m_G(x, \theta)$ exhibits one or several maxima for orientations corresponding to the presence of fibre. Fig. 2.C represents this function for point located in a vertically oriented region, shown as a red cross in Fig. 2.A. The best orientation $\theta^*(x)$, corresponding to the most prominent fibre direction for the pixel x , is computed by integrating the function $m_G(x, \theta)$ over the circular domain $[0; 2\pi[$. The resulting map of orientation is represented using a colour map depending on the orientation: the red colour corresponds to a horizontal orientation, and the light blue colour corresponds to a vertical orientation (Fig. 2.D).

The estimate of local orientation is computed for all pixels. However, as the dark pixels correspond to background, it is relevant to consider only the orientation of the bright pixels. Therefore, parametric maps of local orientation are represented using a colour coding that takes into account both the orientation and the local intensity of the pixel (Fig. 3.C). For the same reason, the histogram of preferred orientations is obtained by computing the histogram of the values $\theta^*(x)$ weighted by $I(x)$, the intensity of x in the original image (Fig. 3.D).

Figure 3.

254 reinforcement is made of continuous individual fibres assembled in 2 mm wide bundles,
255 it is less likely to bend due to its higher moment of inertia compared to flax individual
256 fibres and bundles (Tanguy et al., 2018), with diameters varying from 15 to 100 μm
257 (Charlet et al., 2010; Haag and Müssig, 2016). Also, bundles may have been damaged
258 during the mechanical scutching process and the manufacturing process of unidirectional
259 flax tapes (Khalfallah et al., 2014), where some individual fibres can break up from the
260 bundle and become disoriented, this is visible on Fig. 4.C and 4.F) with some small
261 diameter **bent** fibres. On this point it should be kept in mind that the production of flax
262 fibre reinforcements is a much more complex process than for glass fibres; the glass
263 fibres are extruded and calibrated in an industrial way then directly assembled into roving
264 and preforms. In the case of flax, they are mechanically extracted from a plant, then
265 aligned and ribboned with all the risks involved in these successive operations, with new
266 possibilities for creating defects at each stage.

267 From figure 4. F. it can be observed that on large flax fibre bundles, there is a variation in
268 colour for the same element that can be explained by the fact that the method detects
269 elements crossing each other and for the area where fibres are overlapping, it gives a
270 mean orientation of these later. Also, if the fibres are too wide, the method can hardly
271 recognize them as a single element and thus it gives two symmetric orientations for this
272 element. This later can be resolved by adjusting the image analysis settings with the
273 increase of the morphological filter size which will give a more accurate result but needs
274 a longer time to process.

275 3.2 Application to flax fibre nonwoven preforms

276 **Figure 5.**

277 Similar analyses were performed on flax nonwoven (Figure 5). Referring to the fibre
278 orientation distribution curves, there is a preferred orientation around 90° . This was not
279 reported for glass fibre mats (Fig. 4.G) and this phenomenon can be explained by the

280 manufacturing process of nonwovens which are different for the two materials. Indeed,
281 the glass fibre mat studied here is made by air blowing where fibres are randomly
282 dispersed in the plane whereas flax fibre nonwovens were produced by carding
283 technology with a roller card; fibres are conveyed by several rolls to be disentangled and
284 mixed in order to form homogeneous web of uniform weight per unit area. **Fibres are thus**
285 **more oriented in the machine direction (Van De Velde and Kiekens, 2003). During the**
286 **overlapping step, the web is reoriented almost perpendicularly to the machine direction**
287 **allowing a preferred orientation in the cross direction (CD) (90° in figure 5 and 6). Same**
288 **observations as for unidirectional flaxtape with the fibres overlapping each other can be**
289 **reported for nonwovens.**

290 **Figure 6.**

291 Fig. 6 represents an analysis of the fibre orientation distribution for four different
292 locations on the nonwoven. Trends are found to be quite similar for areas 1, 2 and 3 with
293 a preferred orientation at 90° whereas for the fourth location, the peak is wider and
294 shifted to 70° values and this is likely due to the size of the analysed area. The
295 observation scale is a key point for the accurate analysis of the fibre orientation
296 distribution because if the latter is too small then there are not enough fibres analysed and
297 the distribution thus obtained will not be representative of that of the whole material. On
298 the contrary, if it is too large, the smallest elements may not be detected due to a lack of
299 image quality, leading to an error in determining the orientation of the fibres. With the
300 magnification used here, smaller diameter fibres are detected and by analysing over
301 several areas, it is possible to obtain a precise and representative fibres orientation
302 distribution within the nonwoven. By automating the image analysis, it would then be
303 possible to analyse a very large surface of a sample that can then be mechanically tested
304 and thus verify the actual orientation distribution of the fibres and the impact this will
305 have on the mechanical properties; on the other hand, these data could make it possible to

306 implement a mathematical model to predict the properties of nonwoven composites
307 reinforced by plant fibres. Particular attention should be paid to the fact that with this
308 method, only a surface analysis is performed. This corresponds well for so-called
309 lightweight preforms since the majority of the fibres are analysed here. That said, the
310 increase in weight will affect the thickness of the preform with more fibres in the
311 background that may not have the same orientation as those analysed. **Additionally, in the**
312 **special case of needle-punched nonwovens with higher thickness, the needle punching**
313 **step drives few fibres through the thickness of the material resulting in a three-**
314 **dimensional orientation of the fibres. From these points, a three-dimensional image**
315 **acquisition method and analysis may be required to ensure a reliable fibre orientation**
316 **characterisation on the entire material.**

317

318 **4. Conclusion**

319 This paper presents a new method to analyse the fibre orientation distribution (FOD) of
320 both synthetic and flax preforms for composite reinforcement. Preforms images were
321 obtained by scanning electronic microscopy (SEM) and analysed by computing the
322 histogram of pixels preferred orientations by using gray-level granulometry. Gray-level
323 granulometry is an approach for image texture analysis based on the application of
324 morphological filters (typically opening or closing) of increasing size which results in
325 granulometric curves that can be interpreted in terms of size distribution. The method
326 computes a parametric map of local orientation using a colour coding taking into account
327 both the orientation and the local intensity of the pixel. It also gives a histogram
328 representing the preferred orientations of the analysed elements.

329 Originally developed for flax fibre nonwovens, the method is first validated with more
330 conventional materials such as unidirectional glass fabric, UD flax tapes as well as glass

fibre mat. The results obtained are in accordance with those expected with significant differences between the FOD of the different preforms highlighting the influence of parameters such as the intrinsic characteristics of the materials and their production methods. Similar analyses were performed on different locations of a flax nonwoven which highlighted a preferred orientation around 90°. Due to the reduced size of the analysed area, it is necessary to process to image analysis on different location and arithmetically average the values to assure reliable material fibre orientation distribution.

This method could be combined with several image acquisition techniques (SEM, tomography) both at the preform and composite level offering a large range of applications including composite materials. Potential improvements of the method can be imagined with the quantification fibres and bundles diameters or determination of the orientation in the three dimensions. Finally, it provides interesting perspectives for numerical modelling of biocomposite mechanical properties.

Acknowledgments

The authors would like to thank the French National Association of Research and Technology for funding this work.

References

- Baley, C., Goudenhoof, C., Perré, P., Lu, P., Pierre, F., Bourmaud, A., 2019. Compressive strength of flax fibre bundles within the stem and comparison with unidirectional flax/epoxy composites. *Ind. Crop. Prod.* 130, 25–33. <https://doi.org/10.1016/j.indcrop.2018.12.059>
- Baley, C., Perrot, Y., Busnel, F., Guezenoc, H., Davies, P., 2006. Transverse tensile behaviour of unidirectional plies reinforced with flax fibres. <https://doi.org/10.1016/j.matlet.2006.02.028>
- Bourmaud, A., Beaugrand, J., Shah, D.U., Placet, V., Baley, C., 2018. Towards the design of high-performance plant fibre composites: How can we best define the diversity and specificities of plant cell walls? *Prog. Mater. Sci.* 97, 347–408.

360 <https://doi.org/10.1016/j.pmatsci.2018.05.005>

361 Charlet, K., Jernot, J.P., Eve, S., Gomina, M., Bréard, J., 2010. Multi-scale morphological
362 characterisation of flax: From the stem to the fibrils. *Carbohydr. Polym.* 82, 54–61.
363 <https://doi.org/10.1016/j.carbpol.2010.04.022>

364 Devaux, M.F., Bouchet, B., Legland, D., Guillon, F., Lahaye, M., 2008. Macro-vision
365 and grey level granulometry for quantification of tomato pericarp structure.
366 *Postharvest Biol. Technol.* 47, 199–209.
367 <https://doi.org/10.1016/j.postharvbio.2007.06.017>

368 Eberhardt, C., Clarke, A., 2001. Fibre-orientation measurements in short-glass-fibre
369 composites . Part I: automated , high-angular-resolution measurement by confocal
370 microscopy 61, 1389–1400.

371 Enomae, T., Han, Y.-H., Isogai, A., 2006. Nondestructive determination of fiber
372 orientation distribution of paper surface by image analysis. *Nord. Pulp Pap. Res. J.*
373 21, 253–259. <https://doi.org/10.3183/NPPRJ-2006-21-02-p253-259>

374 Erdman, A., Grzyb, T., Kulpinski, P., Lazarek, J., Lis, S., Olejnik, K., Reczulski, M.,
375 Szczepaniak, P.S., Wysocka-robak, A., 2016. Estimation of Fibre Orientation in
376 Paper Products by an Image Analysis On-line System 2, 107–112.
377 <https://doi.org/10.5604/12303666.1191435>

378 Gager, V., Le Duigou, A., Bourmaud, A., Pierre, F., Behloul, K., Baley, C., 2019.
379 Understanding the effect of moisture variation on the hygromechanical properties of
380 porosity-controlled nonwoven biocomposites. *Polym. Test.* 78, 105944.
381 <https://doi.org/10.1016/j.polymertesting.2019.105944>

382 Ghassemieh, E., Acar, M., Versteeg, H., 2002. Microstructural analysis of non-woven
383 fabrics using scanning electron microscopy and image processing. Part 1:
384 development and verication of the methods. *Proc. IMechE, Part L J. Mater. Des.*
385 *Appl.* 216, 199–207.

386 Gnaba, I., Omrani, F., Wang, P., Soulat, D., Ferreira, M., Vroman, P., Jaouachi, B., 2018.
387 Mechanical behavior of flax/polypropylene commingled nonwoven at dry scale:
388 Influence of process parameters. *Text. Res. J.* 004051751875578.
389 <https://doi.org/10.1177/0040517518755789>

390 Graupner, N., Beckmann, F., Wilde, F., Müssig, J., 2014. Using synchrotron radiation-
391 based micro-computer tomography (SR μ -CT) for the measurement of fibre
392 orientations in cellulose fibre-reinforced polylactide (PLA) composites. *J. Mater.*
393 *Sci.* 49, 450–460. <https://doi.org/10.1007/s10853-013-7724-8>

394 Graupner, N., Ziegmann, G., Wilde, F., Beckmann, F., Müssig, J., 2016. Procedural
395 influences on compression and injection moulded cellulose fibre-reinforced
396 polylactide (PLA) composites: Influence of fibre loading, fibre length, fibre
397 orientation and voids. *Compos. Part A Appl. Sci. Manuf.* 81, 158–171.
398 <https://doi.org/10.1016/j.compositesa.2015.10.040>

399 Haag, K., Müssig, J., 2016. Scatter in tensile properties of flax fibre bundles: influence of
400 determination and calculation of the cross-sectional area. *J. Mater. Sci.* 51, 7907–
401 7917. <https://doi.org/10.1007/s10853-016-0052-z>

402 Jeon, S.-Y., Yu, W.-R., Kim, M.S., Lee, J.S., Kim, J.W., 2014. Predicting the tensile
403 strength of needle-punched nonwoven mats using X-ray computed tomography and
404 a statistical model. *Fibers Polym.* 15, 1202–1210. [https://doi.org/10.1007/s12221-](https://doi.org/10.1007/s12221-014-1202-z)
405 014-1202-z

406 Jones, R.M., 1999. Mechanics of composite materials. *Mech. Compos. Mater.*
407 <https://doi.org/10.1007/BF00611782>

408 Khalfallah, M., Abbès, B., Abbès, F., Guo, Y.Q., Marcel, V., Duval, A., Vanfleteren, F.,
409 Rousseau, F., 2014. Innovative flax tapes reinforced Acrodur biocomposites : A new
410 alternative for automotive applications. *J. Mater.* 64, 116–126.
411 <https://doi.org/10.1016/j.matdes.2014.07.029>

412 Koh, R., Madsen, B., 2018. Strength failure criteria analysis for a flax fibre reinforced
413 composite. *Mech. Mater.* 124, 26–32.
414 <https://doi.org/10.1016/j.mechmat.2018.05.005>

415 Kratmann, K.K., Sutcliffe, M.P.F., Lilleheden, L.T., Pyrz, R., Thomsen, O.T., 2009. A
416 novel image analysis procedure for measuring fibre misalignment in unidirectional
417 fibre composites. *Compos. Sci. Technol.* 69, 228–238.
418 <https://doi.org/10.1016/j.compscitech.2008.10.020>

419 Krause, M., Hausherr, J.M., Burgeth, B., Herrmann, C., Krenkel, W., 2010.
420 Determination of the fibre orientation in composites using the structure tensor and
421 local X-ray transform. *J. Mater. Sci.* 45, 888–896. [https://doi.org/10.1007/s10853-](https://doi.org/10.1007/s10853-009-4016-4)
422 [009-4016-4](https://doi.org/10.1007/s10853-009-4016-4)

423 Legland, D., Devaux, M.F., Bouchet, B., Guillon, F., Lahaye, M., 2012. Cartography of
424 cell morphology in tomato pericarp at the fruit scale. *J. Microsc.* 247, 78–93.
425 <https://doi.org/10.1111/j.1365-2818.2012.03623.x>

426 Luo, G.M., Sadegh, A.M., Cowin, S.C., 1991. The mean intercept length polygons for
427 systems of planar nets. *J. Mater. Sci.* 26, 2389–2396.
428 <https://doi.org/10.1007/BF01130186>

429 Martin, N., Davies, P., Baley, C., 2016. Evaluation of the potential of three non-woven
430 flax fiber reinforcements: Spunlaced, needlepunched and paper process mats. *Ind.*
431 *Crops Prod.* 83, 194–205. <https://doi.org/10.1016/j.indcrop.2015.10.008>

432 Martin, N., Davies, P., Baley, C., 2014. Comparison of the properties of scutched flax
433 and flax tow for composite material reinforcement. *Ind. Crops Prod.* 61, 284–292.
434 <https://doi.org/10.1016/j.indcrop.2014.07.015>

435 Merotte, J., Le Duigou, A., Bourmaud, A., Behlouli, K., Baley, C., 2016. Mechanical and
436 acoustic behaviour of porosity controlled randomly dispersed flax/PP biocomposite.
437 *Polym. Test.* 51, 174–180. <https://doi.org/10.1016/j.polymertesting.2016.03.002>

438 Merotte, J., Le Duigou, A., Kervoelen, A., Bourmaud, A., Behlouli, K., Sire, O., Baley,
439 C., 2018. Flax and hemp nonwoven composites: The contribution of interfacial
440 bonding to improving tensile properties. *Polym. Test.* 66, 303–311.
441 <https://doi.org/10.1016/j.polymertesting.2018.01.019>

442 Miao, M., Shan, M., 2011. Highly aligned flax/polypropylene nonwoven preforms for
443 thermoplastic composites. *Compos. Sci. Technol.* 71, 1713–1718.
444 <https://doi.org/10.1016/j.compscitech.2011.08.001>

445 Mieck, K.-P., Lützkendorf, R., Reussmann, T., 1996. Needle-Punched hybrid nonwovens
446 of flax and ppfibers—textile semiproducts for manufacturing of fiber composites.
447 *Polym. Compos.* 17, 873–878. <https://doi.org/10.1002/pc.10680>

448 Pourdeyhimi, B., Kim, H.S., 2002. Measuring Fiber Orientation in Nonwovens: The
449 Hough Transform. *Text. Res. J.* 72, 803–809.
450 <https://doi.org/10.1177/004051750207200909>

451 Russell, S.J., 2007. Handbook of nonwovens. Woodhead Publishing Limited.

452 Sander, E.A., Barocas, V.H., 2009. Comparison of 2D fiber network orientation
453 measurement methods. *J. Biomed. Mater. Res. - Part A* 88, 322–331.
454 <https://doi.org/10.1002/jbm.a.31847>

455 Shah, D.U., Schubel, P.J., Clifford, M.J., 2013. Can flax replace E-glass in structural
456 composites? A small wind turbine blade case study. *Compos. Part B Eng.* 52, 172–
457 181. <https://doi.org/10.1016/j.compositesb.2013.04.027>

458 Smith, R.A., Nelson, L.J., Xie, N., Fraij, C., Hallett, S.R., 2015. Progress in 3D
459 characterisation and modelling of monolithic carbon-fibre composites. *Insight Non-*
460 *Destructive Test. Cond. Monit.* 57, 131–139.
461 <https://doi.org/10.1784/insi.2014.57.3.131>

462 Soille, P., 2003. Morphological Image Analysis. Springer.

463 Syerko, E., Oter, L., Pawar, A., Binetruy, C., Advani, S.G., Eck, B., 2019. Comparative
464 Study of Methods for the Quantification of Fiber Orientations of Composite
465 Reinforcements, in: 21ème Journées Nationales Sur Les Composites - JNC 21.
466 Bordeaux, pp. 1–9.

467 Tanguy, M., Bourmaud, A., Beaugrand, J., Gaudry, T., Baley, C., 2018. Polypropylene
468 reinforcement with flax or jute fibre; Influence of microstructure and constituents
469 properties on the performance of composite. *Compos. Part B Eng.* 139, 64–74.
470 <https://doi.org/10.1016/j.compositesb.2017.11.061>

471 Thomason, J., Yang, L., Gentles, F., 2017. Characterisation of the Anisotropic
472 Thermoelastic Properties of Natural Fibres for Composite Reinforcement. *Fibers* 5,
473 1–12. <https://doi.org/10.3390/fib5040036>

474 Tunák, M., Antoch, J., 2018. Monitoring homogeneity of textile fiber orientation. *Text.*
475 *Res. J.* 88, 1226–1243. <https://doi.org/10.1177/0040517517698983>

476 Tunák, M., Antoch, J., Kula, J., Chvojka, J., 2014. Estimation of fiber system orientation
477 for nonwoven and nanofibrous layers: Local approach based on image analysis.
478 *Text. Res. J.* 84, 989–1006. <https://doi.org/10.1177/0040517513509852>

479 Van De Velde, K., Kiekens, P., 2003. Effect of Flax/PP Panel Process Parameters on
480 Resulting Composite Properties. *J. Thermoplast. Compos. Mater.* 16, 413–431.
481 <https://doi.org/10.1177/0892705703031637>

482 Van Kempen, G.M.P., Van den Brink, N., Van Vliet, L.J., Van Ginkel, M., Verbeek,
483 P.W., Blonk, H., 1999. The application of a Local Dimensionality Estimator to the
484 analysis of 3-D microscopic network structures, in: Proceedings of the 11th
485 Scandinavian Conference on Image Analysis, Kangerlussuaq, Greenland. pp. 447–
486 455.

487 Yousfani, S.H.S., Gong, R.H., Porat, I., 2012. Manufacturing of Fibreglass Nonwoven
488 Webs Using a Paper Making Method and Study of Fibre Orientation in These Webs.
489 *Fibres Text. East. Eur.* 91, 61–67.

490 Yurgartis, S.W., 1987. Measurement of small angle fiber misalignments in continuous
491 fiber composites. *Compos. Sci. Technol.* 30, 279–293. [https://doi.org/10.1016/0266-](https://doi.org/10.1016/0266-3538(87)90016-9)
492 [3538\(87\)90016-9](https://doi.org/10.1016/0266-3538(87)90016-9)

493

Figure captions

Figure 1. Computation of granulometric curves using morphological opening. Top row: sample results of morphological opening using square structuring elements of increasing sizes. Bottom: resulting granulometric curve. The dots on the curve correspond to the stages shown on the first row.

Figure 2. Computation of preferred orientation map on a synthetic image. A) Original image. B) Results of local mean size for different families of linear structuring element oriented with 0, 45, 90 and 135 degrees. C) Mean size function for a single pixel and the whole range of orientations. D) Synthetic map of preferred orientation represented using colour.

Figure 3. Computation of local orientation map from granulometry curves obtained by analysis on a flax nonwoven. A) Original image (inverted) B) Granulometric size obtained with various orientations of structuring elements C) Colour representation of preferred orientation map. D) Histogram of preferred orientations.

Figure 4. Original SEM images of A) glass fibre mat, B) glass fibre unidirectional preform and C) flax fibre unidirectional tape. D), E) and F) are the computed preferred orientation maps of glass fibre mat, glass UD and flax UD, respectively. G) is the comparison of the fibre orientation distribution (FOD) of the preforms.

Figure 5. Original SEM image of flax fibres nonwoven A). B) is the computed preferred orientation maps of A) and C) shows the histogram representing the fibre orientation distribution.

Figure 6. Original SEM image of a larger area of flax fibres nonwoven divided in four areas A). The histogram represents the fibre orientation distribution of each area analysed B).

Figure 1.

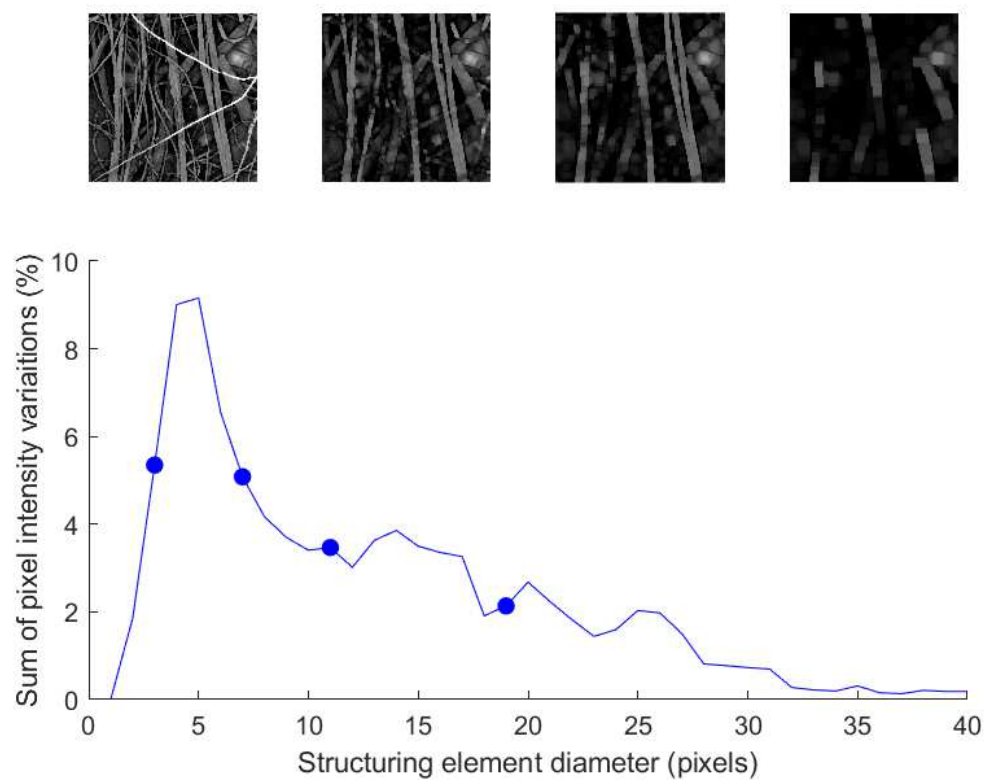


Figure 2.

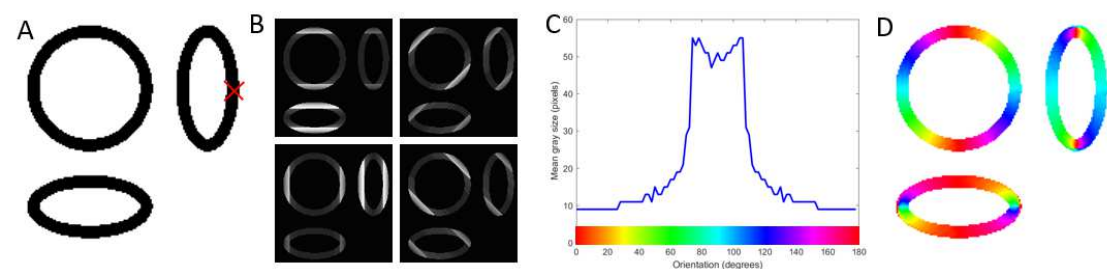


Figure 3.

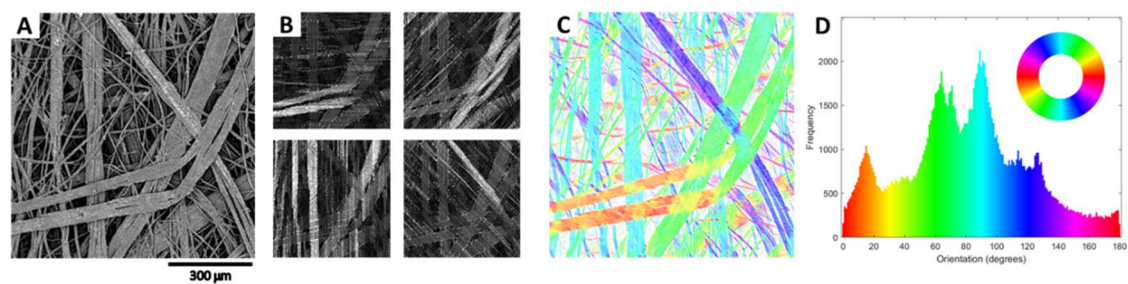


Figure 4.

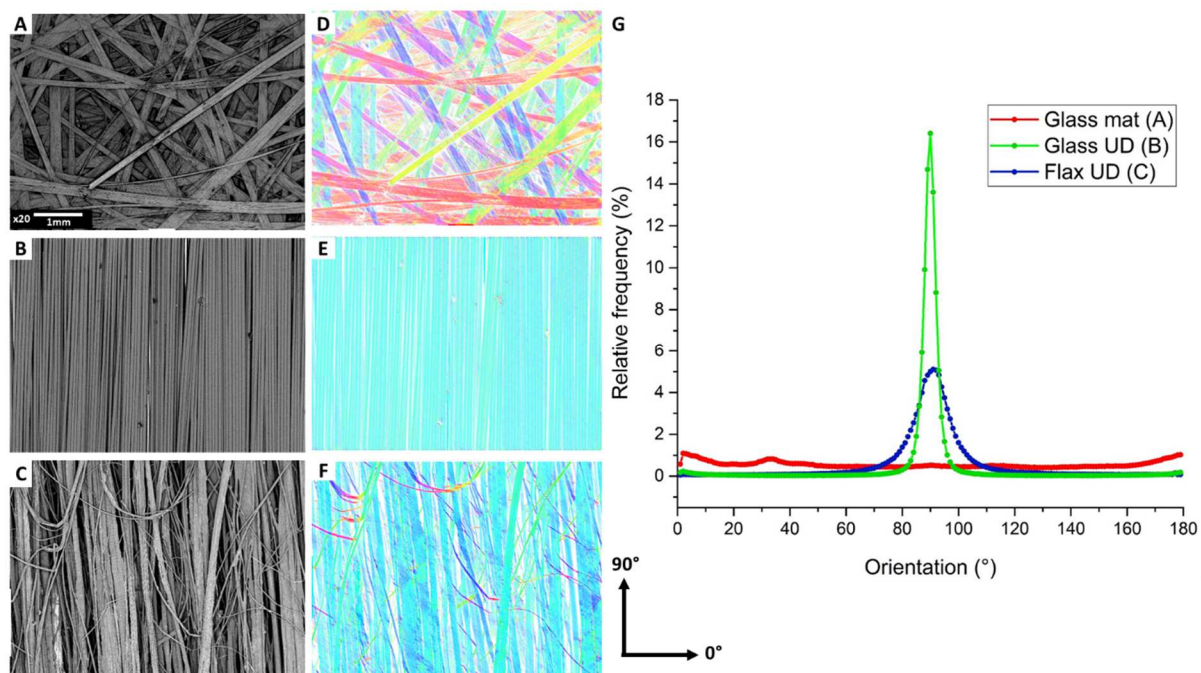


Figure 5.

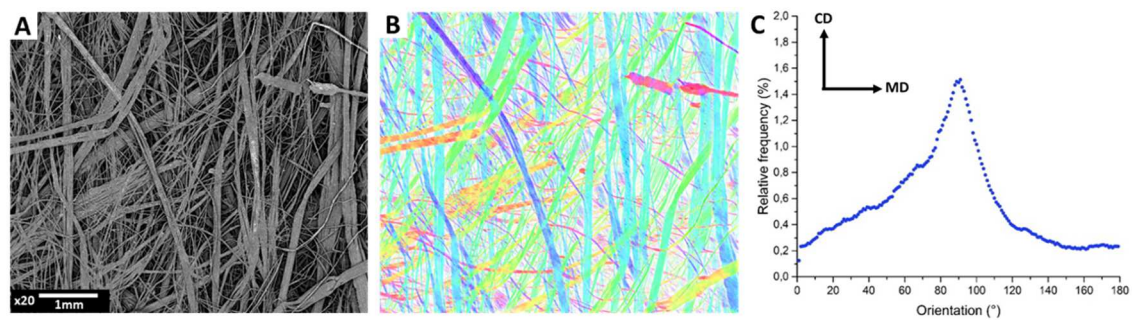


Figure 6.

